WILEY VCH

RESEARCH ARTICLE

Deciphering pH Mismatching at the Electrified Electrode–Electrolyte Interface towards Understanding Intrinsic Water Molecule Oxidation Kinetics

Miao Wang and Ken Sakaushi*

[*] Dr. M. Wang, Prof. Dr. K. Sakaushi
Research Center for Energy and Environmental Materials
National Institute for Materials Science
1-1 Namiki, Tsukuba, Ibaraki 305-0044, Japan
E-mail: *SAKAUSHI.Ken@nims.go.jp*
Webpage: https://www.nims.go.jp/group/eec/en/

Supporting information for this article is given via a link at the end of the document.

Abstract: Unveiling the key influencing factors towards electrode/electrolyte interface control is a long-standing challenge for a better understanding of microscopic electrode kinetics, which is indispensable to building up guiding principles for designer electrocatalysts with desirable functionality. Herein, we exemplify the oxygen evolution reaction (OER) *via* water molecule oxidation with the iridium dioxide electrocatalyst and uncovered the significant mismatching effect of pH between local electrode surface and bulk electrolyte: the intrinsic OER activity under acidic or near-neutral condition was deciphered to be identical by adjusting this pH mismatching. This result indicates that the local pH effect at the electrified solid-liquid interface plays the main role in the "*fake*" OER performance. This local pH effect on the OER electrode process is further verified by integrating a wide spectrum of analytical approaches. This study will accelerate the understanding of the local proton-induced effect on electrode interface processes and the development of advanced electrochemical activity.

Introduction

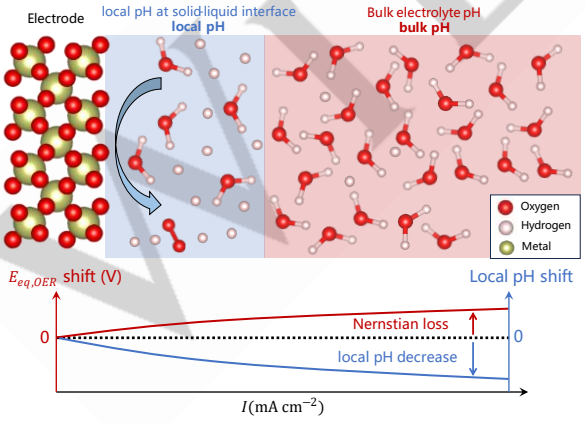

Figure 1. Upon oxygen evolution reaction (OER) with water molecule as the reactant, the local pH at solid-liquid interface (local pH) negatively shifts compared to bulk electrolyte pH (bulk pH) with OER rate increases due to accumulation of protons at the interface. This mismatching between the local and the bulk pH induces a potential mismatching, *i.e.*, the Nernstian loss. Our work elaborates to quantify this Nernstian loss and clarify its influence on OER performance *via* water molecule oxidation.

With growing attention on carbon neutrality, a wide spectrum of electrochemical approaches producing green and sustainable chemicals by combining renewable electricity and aqueous-electrolyte-based energy conversion systems,[1] such as electrolysers,[2] is of great interest in both modern academia and industry communities.[3] For example, the investment in electrolysers will reach USD 5 billion in 2024.[4] As such, water molecule (H_2O) not only acts as solvents in a wide spectrum of electrochemical reactions but also can directly participate in the reactions for the sake of electrified electrode-electrolyte interface.[5] Although the study on electrified electrode-electrolyte interface has initiated by Frumkin in the 1930s and a modern version of microscopic description by Schmickler in the 1980s,[6] many basic aspects in this subject are still yet to be known,[7] such as the structure of interfacial water,[8] the influence of local environment and the relevant electrode reactions,[5b, 9] the interface structure in non-aqueous solvents,[10] the dynamic interface structure away the equilibrium,[11] and complete atomical theoretical descriptions of the interface.[12] One of the most representative questions here lies in the electrochemical water splitting, *id est* (*i.e.*) hydrogen evolution reaction (HER), and oxygen evolution reaction (OER).[13] Especially, the OER is well-known as the bottleneck for the overall water splitting due to its sluggish kinetics with four-electron/proton-transfer steps to release one dioxygen molecule (O_2) from two H_2O.[14] However, its microscopic electrode process is still under debate. Especially, pH mismatching is known to cause misleading interpretation mechanisms or observe "*fake*" electrochemical activities.[9b, 15] As for OER, there are two types of reactants, *i.e.* hydroxides (OH^-) and H_2O.[16] Benefited from the much higher concentration of water molecules (*e.g.*, ~55.6 M in pure water) for promoting the supplementary of reactant, the H_2O path for OER exhibits larger limiting current density as compared to the OH^- path (see a simple comparison in Figure S1 in the Supporting Information (SI)). This makes H_2O path more promising in industrial applications with typically large current densities as compared with lab-scale configurations.[17] However, the accumulated protons during water molecule oxidation gives rise to an additional concentration overpotential, so-called Nernstian loss ($\Delta\varphi_{\text{Nernstian}}$) by following the Nernst Equation

$$\Delta\phi_{Nernstian} = \frac{2.303RT}{F}|pH_{local} - pH_{bulk}|$$

, where *R* is gas constant, *T* is absolute temperature for reaction, *F* is Faraday constant, pH_{local} and pH_{bulk} are local pH in the electrode-electrolyte interface and the pH in the bulk electrolyte, respectively. This energetic loss due to thermodynamic mismatching on potential brings down the energy efficiency of OER, especially significant in a higher current density with a lower local pH for a larger $\Delta\varphi_{Nernstian}$.[15a, 18] Although it is the ultimate goal to establish a comprehensive theoretical model, which is able to let us understand the detailed effects of microscopic reaction environment on electrocatalytic processes with high accuracy and reliability by first-principle calculations and/or modern experimental approaches,[9c, 19] our understanding on microscopic pictures of solid-liquid interfaces is still yet far to achieve this grand challenge. Therefore, in order to advance our understanding on the dominating local pH effect on OER performance and further promote a rational design of a highly efficient anode electrolysis system, a simple but reliable picture of microscopic electrified solid-liquid interfaces described by a combination of experiment and theory is highly demanded.

Herein, we focused on the local pH adjacent to electrode surface for water molecule oxidation towards OER while monitoring the dynamic Nernstian loss (**Figure 1**). We combined microkinetic analyses with *operando* electrochemical methods to reveal the main effect of local pH drift on OER performance. An unconventional reversible hydrogen reference electrode calibrated by local pH was proposed to facilitate an easy understanding of the intrinsic performance of water molecule oxidation for OER. This work shows the crucial roles of not only reactants but also products in electrode-electrolyte interface processes. We hope that this fundamental study will contribute to the elucidation of key effects of the local microenvironment on oxygen electrolysis and promote the development of high-efficiency electrochemistry-based green industries in the future.

Results and Discussion

Given that OH^- in the electrolyte is more competitive than H_2O for OER and to avoid the influence of OH^- path on water molecule oxidation, herein we selected two typical conditions with ultra-low OH^- concentrations, *i.e.* strongly acidic with pH 1 and near-neutral with pH 5, in a three-electrode configuration by loading the benchmark IrO_x on a rotating ring-disk electrode (RRDE). The details are shown in the Experimental Details in the SI. As compared to the acidic condition, the OER *via* water molecule oxidation in the near-neutral condition was observed with a lower activity (**Figure 2**a). The anion or cation effect (except H^+ or OH^-, *i.e.*, the pH effect) should be ignored by using the identical concentration of ClO_4^- or Na^+ in electrolyte. No buffering agents were added to avoid complicating the electrochemical system. As the sake of continuous proton formation due to water molecules to dioxygen gas conversion, we carried out *operando* local pH measurements *via* a RRDE-based method (**Figure 2**b,c, Figure S2 in the SI, more details see the Experimental Details in the SI).

In acid, the local pH at electrode-electrolyte interface reduced with the increase of OER current density (**Figure 2**b), showing an average pH change rate relative to OER current of -0.07 pH mA^{-1} cm^2. Same as the trend observed in acidic OER, the near-neutral condition showed decrease in local pH with increase of OER current density (**Figure 2**c), with an average pH change rate relative to OER current of -0.36 pH mA^{-1} cm^2. This significantly faster pH change rate, as compared to that in acid, could be explained by the much higher sensitivity of pH change to proton concentration change in near-neutral condition than that in acid (Figure S3a in the SI). As a result, just a tiny change of proton concentration on electrode-electrolyte interface could be clearly detected by surface pH change in near-neutral condition during OER. This could be showcased by the obvious decrease in local pH even in the potential range (1.2-1.4 V) with negligible OER current (**Figure 2**c). We ascribed the pH change in this region to the produced protons by redox transition on the electrocatalyst IrO_x.[20] We further conducted error analysis for the RRDE-based pH measurement used in this work (Figure S4 in the SI).

On account of the thermodynamic influence of pH on OER equilibrium potential,[21] we calibrated the reversible hydrogen electrode (RHE) by using the local pH during OER for a clear picture (here marked as $RHE_{local\ pH}$). Surprisingly, we found that the OER activities in acidic and near-neutral conditions were almost identical (**Figure 2**d, more pH conditions see Figure S3b in the SI). This indicated that the different OER activities in a routine comparison (**Figure 2**a) mainly resulted from the local pH-induced equilibrium potential shift of OER, *i.e.*, the thermodynamical influence by local pH shift on OER performance (reaction kinetics). Given the nearly identical intrinsic OER performance between acidic and near-neutral conditions, in the next parts the results in 0.5 M $NaClO_4$, with obvious local pH shifts during reaction, typified the exploration on local pH effects for water molecule oxidation.

To further confirm the local pH effect on OER, first we carried out kinetic analysis by Koutecky-Levich (K-L) equation without considering Nernstian loss (Figure S5 in the SI). We found that the slopes in K-L plot under various potentials were quite different (Figure S5b,5c in the SI). This result was contradictory with the K-L equation that the slope should be constant under different potentials. Such an inconsistency suggested that the change of OER performance under various rotating speeds (Figure S5a in the SI) was not from the mass transport of the reactant (*i.e.*, the water molecules). Thus, we included the Nernstian loss in the above kinetic model (see more in Experimental Details in the SI) and obtained the linear $\frac{1}{i} \sim \frac{i}{\sqrt{\omega}}$ plots (**Figure 2**e) and the nearly unchanged $Slope/e^{\frac{-\alpha FE}{RT}}$ (**Figure 2**f). These results matched with the Nernstian loss-based kinetic model very well, as further evidenced by the linear relationship between 1/*i* and $e^{\frac{-\alpha FE}{RT}} i\ \omega^{-1/2}$ (Figure S5d in the SI). Through the above simple kinetic analyses, we can confirm that the reaction kinetics of water molecule oxidation for OER is dominatingly influenced by Nernstian loss induced by local pH shift because of continuous release of protons.

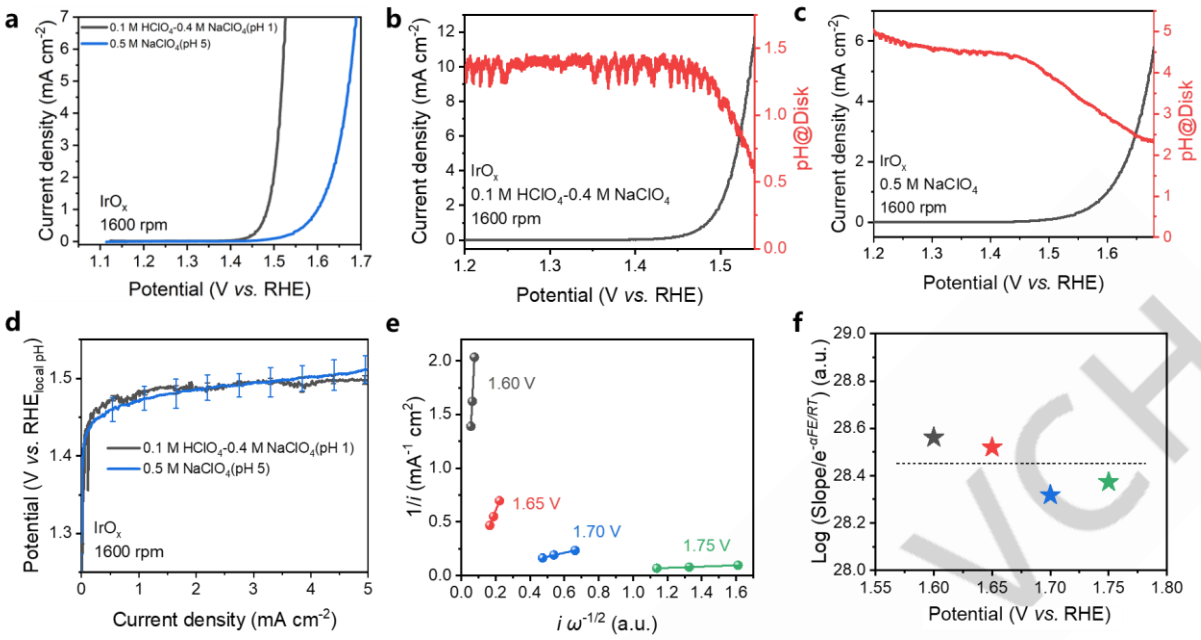

Figure 2. Local pH shift during OER. (a) LSV (1 mV s^{-1}) in acidic and near-neutral conditions for OER at 1600 rpm, and local pH adjacent to the disk electrode in (b) acidic and (c) near-neutral conditions with OER proceeding. (d) Polarization curves for OER in acidic and near-neutral conditions by using local pH-calibrated RHE ($RHE_{local\ pH}$) as the reference electrode, the error bars were obtained by conducting experiments for three times. (e) $1/i - i\,\omega^{-1/2}$ plots at various potentials by the Nernstian loss-based kinetic analysis for OER (0.5 M $NaClO_4$) and (f) the related slope analysis, for more details please refer to the Experimental Details in the SI. The RHE calibrated by bulk electrolyte pH (*i.e.*, $RHE_{bulk\ pH}$) was simplified as RHE.

Based on the above simple kinetic analysis for the local pH-triggered thermodynamic barrier drift (as show in **Figure 3**a), we could envisage a more complicated microkinetic exploration on OER than ever before (see more discussions in Figure S6,S7 and Table S1,S2 in the SI). Thus, instead of the conventional RHE, we turned to use the RHE calibrated by local pH (*i.e.*, $RHE_{local\ pH}$) as the potential reference to favour the understanding of intrinsic water molecule oxidation by fixing the OER equilibrium potential (*i.e.* always 1.23 V under various local pH conditions). To simplify the discussion, herein we used a typical concerted proton-coupled electron transfer (CPET) process to demonstrate the water molecule oxidation for oxygen evolution (**Figure 3**b). The step of formation of *OOH from *O (*O + H_2O → *OOH + H^+ + e^-) was regarded as the rate-determining step (RDS),[22] which will be further verified in the following part. For quantifying the proton concentration during OER, we adopted an empirical equation to describe the relationship between proton concentration and the applied potential (Figure S8 in the SI). As a result, the microkinetic model could overall depict the experimental OER activity (**Figure 3**c, see more details in eq. S12-S24 and Table S3 in the SI), suggesting that the local pH-based microkinetic model for OER should be effective. In the microkinetic analysis, the current density was limited to several milliamperes per square centimetre for avoiding the influence of oxygen bubbles under high current densities on measuring local pH by the RRDE-based method.

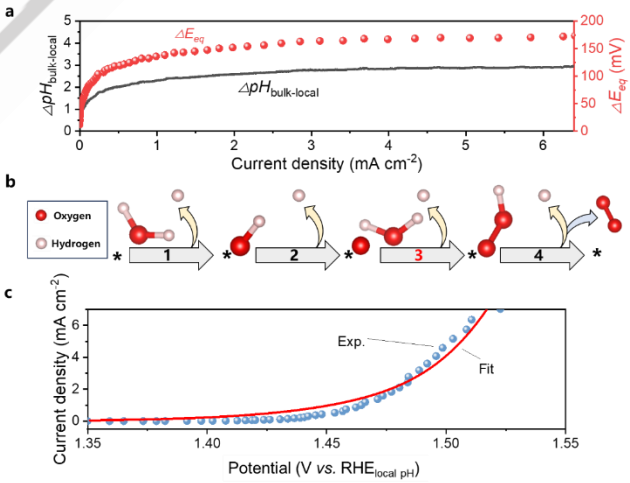

Figure 3. Local pH-based microkinetic analysis for OER in 0.5 M $NaClO_4$. (a) The pH changes between bulk and local electrolyte with increasing the OER current density, as well as the dynamic drift of equilibrium potential for OER. (b) The reaction pathway of water molecule oxidation towards OER, with the 3rd step from *O to *OOH as the RDS. (c) Polarization curve for OER calibrated by local pH and its fitting according to the microkinetic analysis.

To show more evidence for the above microkinetics, we analysed the key reaction intermediate *OH during OER by combining *operando* methods. We transferred the $RHE_{local\ pH}$ to the conventional RHE for comparing with other results (Figure S9 in the SI). As reported in previous studies, the surface reaction intermediate *OH could be readily detected by methanol oxidation reaction (MOR) under electrochemical testing for OER.[23] Thus, in this work we applied this methanol-based method, and found that there was obvious oxidation current of methanol to indicate the surface *OH change (Figure S10a in the SI). The differential current between MOR/OER and OER implied a "volcano" trend of surface *OH with the applied potential (Figure S10b in the SI). To our surprise, this experimentally obtained *OH trend is well consistent with the coverage change modelled by the local pH-based microkinetic analysis (**Figure 4**a). Note that the potential range we chose for comparison from 1.50 V to 1.65 V (*vs.* RHE) is to avoid 1) large errors in microkinetic modelling due to the too low current density (the lower bound 1.50 V) and 2) possible disturbance from oxygen bubbles (the upper bound 1.65 V).

After confirming the consistency of *OH trend between the local pH-based microkinetic analysis and MOR method, we carried out *operando* electrochemical attenuated total reflection-surface-enhanced infrared absorption spectroscopy (ATR-SEIRAS) to obtain more information about adsorption species during water molecule oxidation.[8b, 24] We loaded the pyrolyzed IrO_x powders on the Au-coated Si prism as the working electrode, as the three-electrode configuration shown in **Figure 4**b (see more details in Experimental Details in the SI). The spectra were recorded at a potential range from 0.922 V to 1.958 V (*vs.* RHE), with the result at 0.922 V as the reference. The peaks at 3650 cm^{-1} and around 3500 cm^{-1} were attributable to dangling (*i.e.*, non-hydrogen bonded) water and hydrogen-bonded water, respectively.[8b, 25] It is evident that there was a shift of the peak for hydrogen-bonded water to lower wavenumber with increasing the potential. This red shift could result from the more regular hydrogen bond network of water with oxygen-down orientation by increasing the potential.[8a, 8b] Another possible reason for this red shift might be due to a stronger water-electrode interaction induced by the preferred oxygen-down water molecule with a more positive potential.[26] In addition, the downward peak intensity at around 3500 cm^{-1} kept growing with increasing the potential. This intensity change of the interface water could derive from the replacement of adsorbed water by the produced reaction intermediates (*e.g.*, *OH, *O) from water molecules in the OER reaction pathway, as well as more adsorbed ClO_4^- by increasing the potential (Figure S11 in the SI).[8b] All the above results demonstrate that the water molecules serve as reactants for the electrocatalytic OER, consistent with our (micro)kinetic analyses.

Furthermore, we monitored the trend of *OH (around 2880 cm^{-1} in **Figure 4**c, Figure S12 in the SI) and replotted in **Figure 4**d.[25b, 27] It showed that with increasing the potential, *OH exhibited a "volcano-type" trend. Note that this peak position of *OH plot extracted from the ATR-SEIRAS testing is more positive than that in **Figure 4**a. We attributed this difference to the different proton diffusion conditions: the lower surface proton concentration in the rotating electrode system (**Figure 4**a) lead to smaller Nernstian loss for the more negative potential with respect to RHE towards OER, as compared with the higher surface proton concentration in the static system (**Figure 4**b) due to the slower proton diffusion. Therefore, together with MeOH-based approach, the spectroscopy-detected *OH trend solidifies our (micro)kinetic results for the thermodynamic barrier induced by local pH shift.

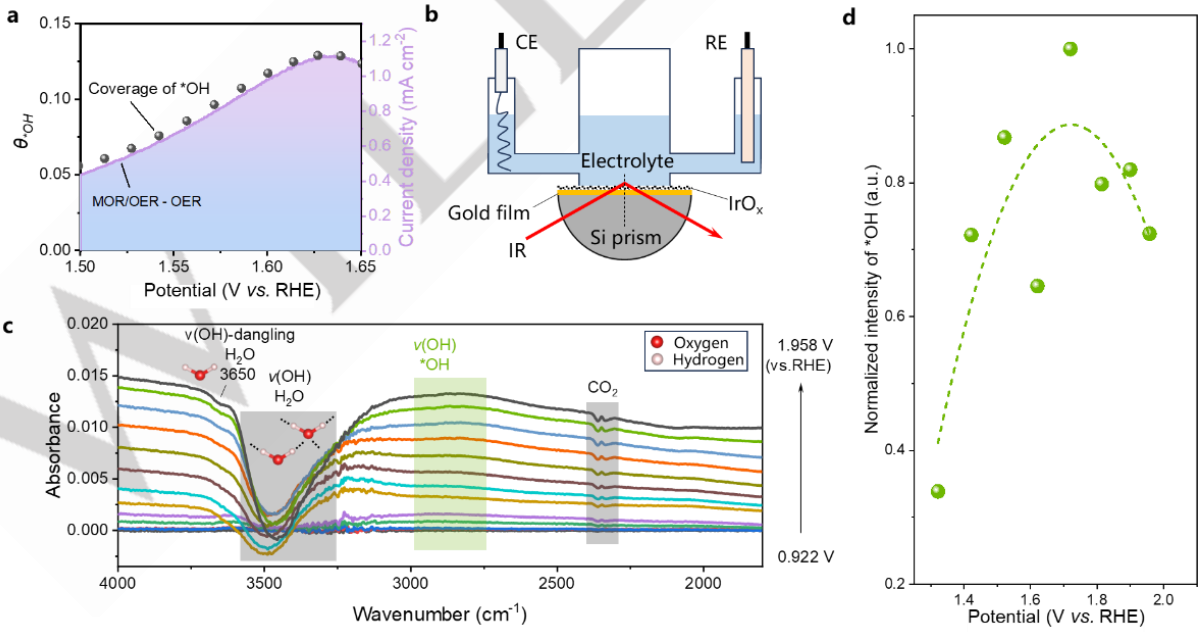

Figure 4. Monitoring *OH during water molecule oxidation in 0.5 M $NaClO_4$. (a) Trends of coverage of *OH by local pH-based microkinetic modelling and MOR detection. (b) The electrochemical configuration for *operando* SEIRAS and (c) the spectra with increasing the potential, reference spectroscopy: 0.922 V (*vs.* RHE). (d) The trend of *OH amount detected by ATR-SEIRAS with increasing the potential.

Conclusion

In this work, we revealed the local pH effect at electrode-electrolyte interface on water molecule oxidation for electrocatalytic OER performance. The main effect was experimentally evidenced to be the Nernstian loss, *i.e.*, the dynamic drift of equilibrium potential for OER with the reaction current density changing. By combining microkinetic analyses and *operando* electrochemical approaches, we further explored the local pH effect-included electrode process with the formation of a reaction intermediate *OOH as the rate-determining step. In addition, different from the conventional RHE calibrated by bulk pH of electrolyte, we proposed an unconventional RHE, *i.e*. the reversible hydrogen reference electrode calibrated by local pH on the electrocatalyst surface, to benefit the clarification of intrinsic performance of water molecule oxidation towards OER. We believe that our fundamental study on local pH effect on electrode-electrolyte interface will promote the understanding of protic-solvent-based microscopic electrode processes and contribute to the exploration of highly efficient renewable power-to-X systems in the future.

Supporting Information

The authors have cited additional references within the Supporting Information.[8b, 9c, 16a, 19b, 25b, 28]

Acknowledgements

KS and MW are indebted to the National Institute for Materials Science. This work was partially supported by GteX Program Japan Grant Number JPMJGX23H2.

Conflict of Interest

The authors declare no conflict of interest.

Data Availability Statement

The data that support the findings of this study are available from the corresponding author upon reasonable request.

Keywords: Electrocatalysis • Water molecule oxidation • Local pH effect • Microkinetics • Electrified electrode-electrolyte interface

[1] Z. W. Seh, J. Kibsgaard, C. F. Dickens, I. Chorkendorff, J. K. Nørskov, T. F. Jaramillo, *Science* **2017**, *355*, eaad4998.

[2] M. Chatenet, B. G. Pollet, D. R. Dekel, F. Dionigi, J. Deseure, P. Millet, R. D. Braatz, M. Z. Bazant, M. Eikerling, I. Staffell, P. Balcombe, Y. Shao-Horn, H. Schäfer, *Chemical Society Reviews* **2022**, *51*, 4583-4762.

[3] R. Daiyan, I. MacGill, R. Amal, *ACS Energy Letters* **2020**, *5*, 3843-3847.

[4] IEA, International Energy Agency (IEA), Paris, **2024**.

[5] a) R. Parsons, *Chemical Reviews* **1990**, *90*, 813-826; b) T. Kumeda, K. Sakaushi, *Current Opinion in Electrochemistry* **2022**, *36*, 101121.

[6] a) H. Helmholtz, *Annalen der Physik* **1879**, *243*, 337-382; b) M. Gouy, *J. Phys. Theor. Appl.* **1910**, *9*, 457-468; c) D. L. Chapman, *The London, Edinburgh, and Dublin Philosophical Magazine and Journal of Science* **1913**, *25*, 475-481; d) O. Stern, *Zeitschrift für Elektrochemie und angewandte physikalische Chemie* **1924**, *30*, 508-516; e) R. Oscar Knefler, *Physical Review* **1928**, *31*, 1051-1059; f) A. Frumkin, *Zeitschrift für Physikalische Chemie* **1933**, *164A*, 121-133; g) D. C. Grahame, *Chemical Reviews* **1947**, *41*, 441-501; h) W. Schmickler, *Journal of Electroanalytical Chemistry and Interfacial Electrochemistry* **1983**, *150*, 19-24.

[7] V. R. Stamenkovic, D. Strmcnik, P. P. Lopes, N. M. Markovic, *Nature Materials* **2017**, *16*, 57-69.

[8] a) M. F. Toney, J. N. Howard, J. Richer, G. L. Borges, J. G. Gordon, O. R. Melroy, D. G. Wiesler, D. Yee, L. B. Sorensen, *Nature* **1994**, *368*, 444-446; b) K.-i. Ataka, T. Yotsuyanagi, M. Osawa, *The Journal of Physical Chemistry* **1996**, *100*, 10664-10672; c) Y.-H. Wang, S. Zheng, W.-M. Yang, R.-Y. Zhou, Q.-F. He, P. Radjenovic, J.-C. Dong, S. Li, J. Zheng, Z.-L. Yang, G. Attard, F. Pan, Z.-Q. Tian, J.-F. Li, *Nature* **2021**, *600*, 81-85.

[9] a) E. L. DeWalt-Kerian, S. Kim, M. S. Azam, H. Zeng, Q. Liu, J. M. Gibbs, *The Journal of Physical Chemistry Letters* **2017**, *8*, 2855-2861; b) W. Chen, M.-K. Zhang, B.-Y. Liu, J. Cai, Y.-X. Chen, *Current Opinion in Electrochemistry* **2022**, *34*, 101003; c) X. Zhu, J. Huang, M. Eikerling, *Accounts of Chemical Research* **2024**, *57*, 2080-2092.

[10] a) A. A. Kornyshev, R. Qiao, *The Journal of Physical Chemistry C* **2014**, *118*, 18285-18290; b) R. Hayes, G. G. Warr, R. Atkin, *Chemical Reviews* **2015**, *115*, 6357-6426.

[11] Z. Zhang, Y. Gao, S. Chen, J. Huang, *Journal of The Electrochemical Society* **2020**, *167*, 013519.

[12] a) M. H. Hansen, A. Nilsson, J. Rossmeisl, *Physical Chemistry Chemical Physics* **2017**, *19*, 23505-23514; b) A. Groß, S. Sakong, *Current Opinion in Electrochemistry* **2019**, *14*, 1-6.

[13] a) Nicholson, Carlisle, Cruickshank, *The Philosophical Magazine* **1800**, *7*, 337-347; b) A. Fujishima, K. Honda, *Nature* **1972**, *238*, 37-38; c) T. Shinagawa, A. T. Garcia-Esparza, K. Takanabe, *Scientific Reports* **2015**, *5*, 13801; d) W. Hoisang, K. Sakaushi, *Current Opinion in Electrochemistry* **2022**, *36*, 101136.

[14] a) J. O. M. Bockris, *The Journal of Chemical Physics* **1956**, *24*, 817-827; b) M. W. Kanan, D. G. Nocera, *Science* **2008**, *321*, 1072-1075; c) E. Fabbri, T. J. Schmidt, *ACS Catalysis* **2018**, *8*, 9765-9774.

[15] a) M. R. Singh, E. L. Clark, A. T. Bell, *Physical Chemistry Chemical Physics* **2015**, *17*, 18924-18936; b) M.-K. Zhang, Z. Wei, W. Chen, M.-L. Xu, J. Cai, Y.-X. Chen, *Electrochimica Acta* **2020**, *363*, 137160.

[16] a) T. Nishimoto, T. Shinagawa, T. Naito, K. Takanabe, *Journal of Catalysis* **2020**, *391*, 435-445; b) T. Nishimoto, T. Shinagawa, T. Naito, K. Takanabe, *ChemSusChem* **2021**, *14*, 1554-1564.

[17] T. Lazaridis, B. M. Stühmeier, H. A. Gasteiger, H. A. El-Sayed, *Nature Catalysis* **2022**, *5*, 363-373.

[18] a) N. Ibl, *Pure and Applied Chemistry* **1981**, *53*, 1827-1840; b) Y. Yokoyama, T. Fukutsuka, K. Miyazaki, T. Abe, *Journal of The Electrochemical Society* **2018**, *165*, A3299; c) T. Naito, T. Shinagawa, T. Nishimoto, K. Takanabe, *ChemSusChem* **2020**, *13*, 5921-5933; d) J. C. Fornaciari, L.-C. Weng, S. M. Alia, C. Zhan, T. A. Pham, A. T. Bell, T. Ogitsu, N. Danilovic, A. Z. Weber, *Electrochimica Acta* **2022**, *405*, 139810.

[19] a) X. Zhu, J. Huang, M. Eikerling, *JACS Au* **2023**, *3*, 1052-1064; b) J. Huang, *The Journal of Chemical Physics* **2020**, *153*, 164707.

[20] C. Liang, R. R. Rao, K. L. Svane, J. H. L. Hadden, B. Moss, S. B. Scott, M. Sachs, J. Murawski, A. M. Frandsen, D. J. Riley, M. P. Ryan, J. Rossmeisl, J. R. Durrant, I. E. L. Stephens, *Nature Catalysis* **2024**, *7*, 763-775.

[21] C. S. Cha, H. L. Huang, Q. Wang, J. T. Lu, L. Zhuang, *Chemical Journal of Chinese Universities* **2008**, *29*, 2479-2483.

[22] Y. Hao, Y. Kang, S. Wang, Z. Chen, C. Lei, X. Cao, L. Chen, Y. Li, Z. Liu, M. Gong, *Angewandte Chemie International Edition* **2023**, *62*, e202303200.

[23] a) H. B. Tao, Y. Xu, X. Huang, J. Chen, L. Pei, J. Zhang, J. G. Chen, B. Liu, *Joule* **2019**, *3*, 1498-1509; b) M. Wang, Y.-S. Wei, L. Zou, H.-F. Wang, S. Shen, Q. Xu, *The Journal of Physical Chemistry C* **2021**, *125*, 16420-16427.

[24] a) A. Hartstein, J. R. Kirtley, J. C. Tsang, *Physical Review Letters* **1980**, *45*, 201-204; b) M. Osawa, K.-i. Ataka, K. Yoshii, T. Yotsuyanagi, *Journal of Electron Spectroscopy and Related Phenomena* **1993**, *64-65*, 371-379; c) K. Sakaushi, T. Kumeda, S. Hammes-Schiffer, M. M. Melander, O. Sugino, *Physical Chemistry Chemical Physics* **2020**, *22*, 19401-19442.

[25] a) M. Osawa, M. Tsushima, H. Mogami, G. Samjeské, A. Yamakata, *The Journal of Physical Chemistry C* **2008**, *112*, 4248-4256; b) H. Wang, H. D. Abruña, *Journal of the American Chemical Society* **2023**, *145*, 18439-18446; c) N. Sagawa, T. Shikata, *The Journal of Physical Chemistry B* **2015**, *119*, 8087-8095.

[26] Z.-Q. Tian, B. Ren, Y.-X. Chen, S.-Z. Zou, B.-W. Mao, *Journal of the Chemical Society, Faraday Transactions* **1996**, *92*, 3829-3838.

[27] A. Michaelides, P. Hu, *The Journal of Chemical Physics* **2001**, *114*, 513-519.

[28] a) W. J. Albery, E. J. Calvo, *Journal of the Chemical Society, Faraday Transactions 1: Physical Chemistry in Condensed Phases* **1983**, *79*, 2583-2596; b) S. Yao, M. Wang, M. Madou, *Journal of The Electrochemical Society* **2001**, *148*, H29; c) Y. Yokoyama, K. Miyazaki, Y. Miyahara, T. Fukutsuka, T. Abe, *ChemElectroChem* **2019**, *6*, 4750-4756; d) Y. Yokoyama, K. Miyazaki, Y. Kondo, Y. Miyahara, T. Fukutsuka, T. Abe, *Chemistry Letters* **2020**, *49*, 195-198; e) J. H. Wang, *The Journal of Physical Chemistry* **1965**, *69*, 4412-4412; f) T. Shinagawa, M. T.-K. Ng, K. Takanabe, *ChemSusChem* **2017**, *10*, 4155-4162; g) J. O'M Bockris, A. K. N. Reddy, M. Gamboa-Aldeco, *MODERN ELECTROCHEMISTRY, Vol. 2A*, Kluwer Academic, New York, **2000**; h) M. C. O. Monteiro, M. T. M. Koper, *Current Opinion in Electrochemistry* **2021**, *25*, 100649; i) M. C. O. Monteiro, X. Liu, B. J. L. Hagedoorn, D. D. Snabilié, M. T. M. Koper, *ChemElectroChem* **2022**, *9*, e202101223; j) M. H. Hicks, W. Nie, A. E. Boehme, H. A. Atwater, T. Agapie, J. C. Peters, *Journal of the American Chemical Society* **2024**, *146*, 25282-25289; k) J. Huang, M. Li, M. J. Eslamibidgoli, M. Eikerling, A. Groß, *JACS Au* **2021**, *1*, 1752-1765; l) S. S. Veroneau, A. C. Hartnett, J. Ryu, H. Hong, C. Costentin, D. G. Nocera, *Journal of the American Chemical Society* **2024**, *146*, 28925-28931; m) R. L. Doyle, I. J. Godwin, M. P. Brandon, M. E. G. Lyons, *Physical Chemistry Chemical Physics* **2013**, *15*, 13737-13783.

Entry for the Table of Contents

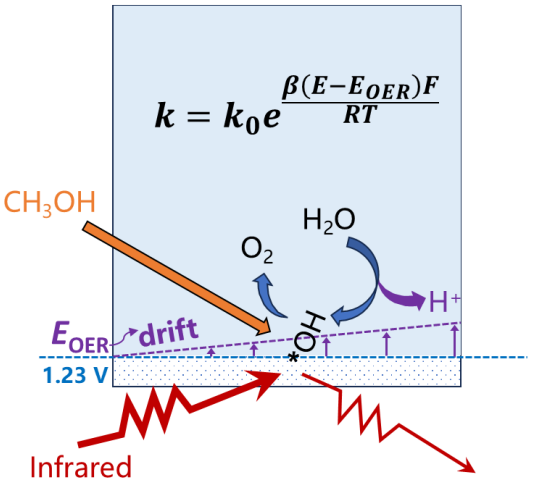

By integrating operando electrochemical methods with (micro)kinetic modelling, the dynamic local pH effect for the oxygen evolution reaction is clarified. An unconventional reversible hydrogen reference electrode is employed, enabling a clearer interpretation of intrinsic electrochemical kinetics. This approach offers deeper insights into the microscopic electrode processes in the electrified electrode-electrolyte interface with dynamic local pH.